energies

MDPI

Article

Predicting Photovoltaic Module Lifespan Based on Combined Stress Tests and Latent Heat Analysis

Woojun Nam [1], Jinho Choi [1], Gyugwang Kim [1], Jinhee Hyun [1], Hyungkeun Ahn [1] and Neungsoo Park [2,*]

[1] Next Generation Photovoltaic Module and Power System Research Center, Konkuk University, Seoul 05029, Republic of Korea; ska4034@cbtp.or.kr (W.N.); jhchoi@cbtp.or.kr (J.C.); rbrhkd00@cbtp.or.kr (G.K.); l6ky4122@konkuk.ac.kr (J.H.); hkahn@konkuk.ac.kr (H.A.)
[2] The Department of Computer Science & Engineering, Konkuk University, Seoul 05029, Republic of Korea
* Correspondence: neungsoo@konkuk.ac.kr

Abstract: In this study, long-term reliability tests for high-power-density photovoltaic (PV) modules were introduced and analyzed in accordance with IEC 61215 and light-combined damp heat cycles, such as DIN 75220. The results indicated that post light soaking procedure, light-combined damp heat cycles caused a 3.51% power drop, while IEC standard tests (DH1000 and TC200) caused only 0.87% and 1.32% power drops, respectively. IEC 61215 failed to assess the long-term reliability of the high-power-density PV module, such as the passivated emitter rear cell. Additionally, based on the combined test, the latent heat (Q_{mod}) of the module was introduced to predict its degradation rate and to fit the prediction curve of the product guaranteed by the PV module manufacturers. Q_{mod} facilitates in predicting a PV module's lifespan according to the environmental factors of the actual installation area. The Q_{mod} values of the PV stations in water environments, such as floating and/or marine PVs, indicated that they would last 7.2 years more than those on a rooftop, assuming that latent heat is the only cause of deterioration. Therefore, extending module life and improving power generation efficiency by determining installation sites to minimize latent heat would be advantageous.

Keywords: degradation rate; latent heat; lifespan of high-power-density module; light-combined damp heat cycles

Academic Editor: Jiaqiang E

Received: 2 December 2024
Revised: 4 January 2025
Accepted: 7 January 2025
Published: 11 January 2025

Citation: Nam, W.; Choi, J.; Kim, G.; Hyun, J.; Ahn, H.; Park, N. Predicting Photovoltaic Module Lifespan Based on Combined Stress Tests and Latent Heat Analysis. *Energies* **2025**, *18*, 304. https://doi.org/10.3390/en18020304

1. Introduction

Among the solar cell manufacturing technologies for high-efficiency solar cells, passivated emitter rear cell (PERC) technology has attracted attention as a core technology. The PERC was first proposed by the University of New South Wales in 1984 [1]. In 1990, a PERC with 20% efficiency was first produced [2]. PERC technology allows solar cell manufacturers to produce Al-BSF solar cells with high solar cell efficiency by simply adding several processes to existing production facilities without large-scale capital investment. However, PERCs using p-type wafers exhibit substantial degradation owing to light-induced degradation (LID) [3]. The LID problem results in an extended time for the incorporation of these cells into mass production. LID is a phenomenon in which the output of solar cells is reduced by solar energy and sunlight, and degradation of the module occurs in the first few hours of exposure to the sun. LID can be divided into boron–oxygen-complex-induced LID (BO-LID) and light- and elevated-temperature-induced degradation (LeTID) [4]. BO-LID is typically observed in boron-doped p-type wafers because oxygen penetrates the ingot and combines with boron during the doping process. A single-crystal ingot is grown in a silica crucible, which does not completely block oxygen diffusion. Therefore, BO-LID is

more likely to occur in crystalline cells than in multicrystalline (mc) cells, which have less structural contact with oxygen. BO-LID can be mitigated by irradiating ingots with light sources, such as lasers, halogens, and LEDs, using light-induced regeneration (LIR) [5]. LeTID occurs when the combination of boron and oxygen is induced by light and heat [6]. After LeTID was discovered in p-type Czochralski (Cz) silicon solar cells in 2017 [7], it was also reported in n-type float-zone (Fz) monocrystalline solar cells [8]. LID occurs in both monocrystalline and multicrystalline PV modules [9]. The degradation rates of multicrystalline modules, namely, mc-BSF and mc-PERC, increased with time [10]. In contrast, monocrystalline modules, namely, Cz-PERC and cast-mono PERC, stabilized at approximately 1.5% [11]. The LID in the multicrystalline PERC increased as the temperature increased [12].

To alleviate LeTID, various methods, such as using the gettering effect, adjusting the wafer thickness, and changing the firing temperature, have been attempted [13]. However, the latest PV modules still experience LeTID [14] because they are likely to generate power at high temperatures owing to their high short-circuit currents [15].

To a certain extent, LID can occur in monocrystalline solar cells. In particular, it is highly likely to occur in PERCs [16], which have rapidly emerged as mainstream high-power PV modules. TOPCon and HJT tandem solar cell technologies have been developed [17], both of which use phosphorus-doped n-type wafers [18]. n-Type TOPCon cells offer high efficiency potential owing to their superior passivation [19], long lifespan owing to the resistance of n-type Cz-Si wafers to metal impurities, and compatibility with existing PERC equipment [20]. After LID testing, TOPCon and HJT tandem cells showed a 0.5% power increase [21], while the power of P-type cells decreased by 5% [22].

The 2024 International Technology Roadmap for Photovoltaics (ITRPV) indicates that PERX technologies, encompassing PERC, PERT, and PERL, will collectively capture nearly 40% of the solar cell market share in 2024. The share of n-TOPCON cells is expected to increase steadily, reaching approximately 60% by 2031. In addition, BSF cells are expected to become obsolete by 2025 [23].

Wafers gradually increased in size from M0. Currently, wafers between M6 and G12 are mixed in use; however, M10 wafers are expected to comprise the majority of wafers. One module manufacturer recently introduced 700 W modules using G12 wafers. At present, high-power modules formed by the partitioning and gathering of enlarged monocrystalline solar PERCs are mainstream. This method is largely divided into shingling and gapless methods, both of which show that the operating temperature is higher than that of normal PV modules. Thus, the conditions for LeTID can be created more easily through the solar cell arrangement method to increase the maximum output of the PERC module.

Although the manufacturing technology for solar cells and PV modules continues to evolve, formal international standards for evaluating the lifetime of PV modules have not yet been established. IEC61215-2, the representative test standard for PV modules, maintained most of its specifications at the time of its enactment in 2006. IEC61215-2 has only been revised to integrate individual test standards into one for thermal phenomena that has been issued [24]. PV modules are products that combine various components [25]. Thus, rather than assessing each material-specific deterioration factor individually, long-term reliability should be evaluated under complex test conditions. In this study, the reliability test specifications of other industries are introduced, and a method for measuring the lifespan of a PV module is proposed based on the test results.

2. Research Background

A typical test specification for evaluating the reliability of monocrystalline PV modules is IEC 61215. This standard was established in 2006 and amended once in IEC 61215:2016.

Another revision of the standard is discussed in IEC 61215:2019. A cyclic (dynamic) mechanical load test (MQT 20), potential-induced degradation test (PID) (MQT 21), bending test (MQT 22) for flexible modules, and LeTID detection test (MQT 23) were added, and the two tests related to the nominal module operating temperature (NMOT) were removed. With these changes, most of the contents regarding the temperature and humidity of chamber testing, which can be used to evaluate the long-term reliability of a monocrystalline PV module, remained the same. Module life is commonly guaranteed to be more than 25 years because manufacturing technology has improved. Therefore, PV module manufacturers have doubled and tripled the number of thermal cycling tests and high-temperature and high-humidity tests in the IEC 61215 test standards to ensure the minimum output characteristics of the module. There are also test standards similar to IEC 61215, such as UL1703 in North America and CQC in China. However, long-term reliability tests conducted without considering the combined effects of UV radiation on polymer materials may not be sufficient for assessing the life of PV modules. Even with the application of the revised IEC 61215:2019, the performance and durability of a module is tested using a separate LeTID detection test (MQT 23) along with IEC 61215 to evaluate the deterioration of PERCs. Long-term reliability tests exist in many names, such as the Long-Term Sequential Test from TÜV Rheinland, Köln, Germany; ATLAS 25 Plus from ATLAS, Austin, TX, USA; and the Test-to Failure Protocol from NREL, Golden, CO, USA.

Table 1 compares the test conditions specified in the IEC 61215 and DIN 75520 standards. IEC 61215 mandates damp heat (DH) and thermal cycle (TC) tests. The DH test exposes the module to a controlled environment of 85 °C and 85% relative humidity for a duration of 1000 h. The TC test subjects the module to a temperature cycling regimen between −40 °C and 80 °C, with TC200 requiring a total test duration of 800 h. Notably, neither the DH test nor the TC test involved solar irradiation. DIN 75520 stipulates dry–humid cycle tests. The dry cycle test subjects the module to a temperature range of 10 °C to 65 °C, a relative humidity below 30%, and an irradiance level of 830 W/m^2 for a total of 360 h. The humid cycle test, in contrast, exposes the module to a temperature range of −10 °C to 65 °C, a relative humidity above 50%, and an irradiance level of 830 W/m^2 for 240 h.

Table 1. Comparison of durability test conditions.

Test		Temp [°C]		Humidity [%]	Irradiance [W/m^2]	Time [h]
		Condition	ΔT	Condition		
IEC 61215	Damp Heat	85	-	85	N/A	1000
	Thermal Cycling	−40–80	120	N/A	N/A	800
DIN 75220	Dry Cycle	10–65	55	<30	830	360
	Humid Cycle	−10–65	75	Condensation ~>50		240

2.1. IEC 61215

Example test results of a high-temperature and high-humidity test of a shingled module made of PERCs are as follows: the test was conducted for 1000 h at 85 °C and 85% relative humidity (RH) conditions after 5 kWh of light soaking, as shown in Figure 1.

The output degradation rates and the initial measured values were 2.48% and 0.87% compared with the measured values after light soaking. As shown in Figure 1 and as listed in Table 2, the results of the high-temperature and high-humidity test indicated a drop rate of 0.87% after light soaking, and this result allowed the module to pass the test with excellent performance.

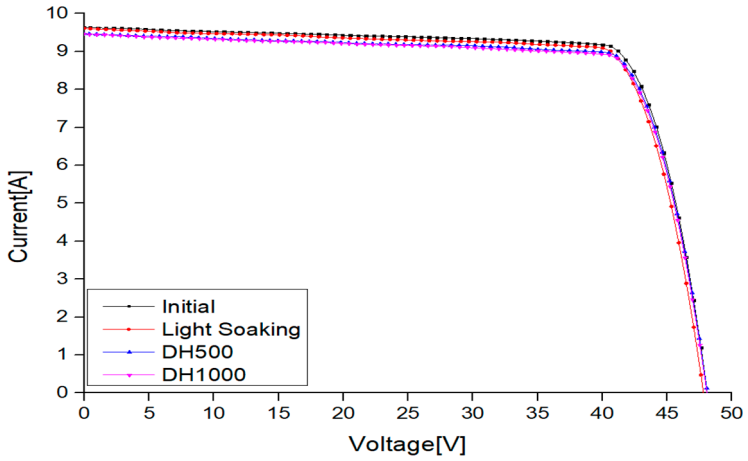

Figure 1. Measured results of the high-temperature and high-humidity test in IEC 61215 (85 °C, 85% RH conditions, 1000 h).

Table 2. Measured data and output degradation rate of the high-temperature and -humidity test in IEC 61215 (85 °C, 85% RH conditions, 1000 h).

	Isc [A]	Voc [V]	Vpm [V]	Ipm [A]	Pm [W]	Rate 1 [%]	Rate 2 [%]
Initial	9.636	48.110	40.941	9.089	372.132	0.00	/
Light Soaking	9.610	47.817	40.583	9.022	366.116	−1.62	−0.00
DH500	9.469	48.112	41.002	8.903	365.046	−1.90	−0.29
DH1000	9.460	48.075	41.015	8.848	362.922	−2.48	−0.87

Thermal cycling tests were conducted after light soaking. The current was applied only to the temperature-rise section with a temperature change of −40 °C to 80 °C. Rate 1 in Table 3 is the degradation rate compared to the initial measured value, and Rate 2 is the degradation rate relative to the value after light soaking.

Table 3. Measured data and output degradation rate of the thermal cycling test in IEC 61215 (−40 to 85 °C, 200 cycles).

	Isc [A]	Voc [V]	Vpm [V]	Ipm [A]	Pm [W]	Rate 1 [%]	Rate 2 [%]
Initial	9.636	48.066	40.950	9.078	371.741	0.00	/
Light Soaking	9.571	47.776	40.584	9.025	366.272	−1.47	0.00
TC100	9.548	47.830	40.431	9.005	364.058	−2.07	−0.60
TC200	9.573	47.863	40.123	9.008	361.427	−2.77	−1.32

After the test, Rate 1 and Rate 2 were measured, with values of 2.77% and 1.32%, respectively. This implies that the module passed the test. A thermal cycling test was designed to examine the durability of the PV module against stresses that occur owing to repeated temperature changes. The I–V curves of the solar module, both before and after light soaking, and the subsequent TC100 and TC200 tests are shown in Figure 2. A more pronounced decrease in current was observed following light soaking than in the modules subjected to the TC100 and TC200 tests. Although the TC test, as outlined in IEC61215, is essential, the reliability evaluation of PERC modules necessitates the consideration of LID. Thus, light soaking tests are imperative for a comprehensive assessment.

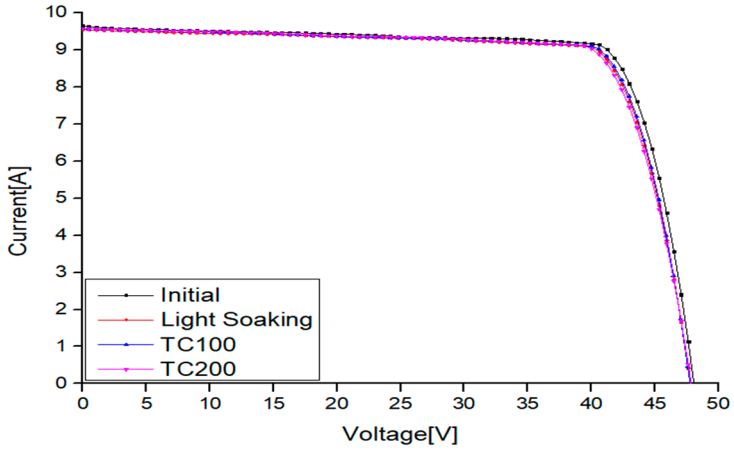

Figure 2. Measured results of the thermal cycling test in IEC61215 (−40 to 85 °C, 200 cycles).

PERX technologies are currently widespread in the market [16]. Therefore, long-term reliability under light-combined conditions should be evaluated rather than LID tests being conducted separately. Thus, a reliability test standard for automobile manufacturers that has long been tested with a combination of solar light, temperature, and humidity (DIN 75220) was applied to the PV modules.

2.2. DIN 75220

DIN 75220 is a testing standard established by the Deutsche Institute für Normung (Figure 3). The test, which was created in 1992 and has been in use since then, ages automobile components in solar simulation units using a solar simulator [26]. The purpose of this test is to evaluate the long-term reliability of automotive interior components by simulating the parts of the polymer material that are deteriorated by solar energy. Although this test is often used to evaluate samples made of a single material, it can also identify the interactions between each component of a sample made of various materials. Therefore, this test is suitable for PV modules composed of various materials. The wavelength of the artificial light source, which is the main component of DIN 75220, was defined differently from that of the PV test standard.

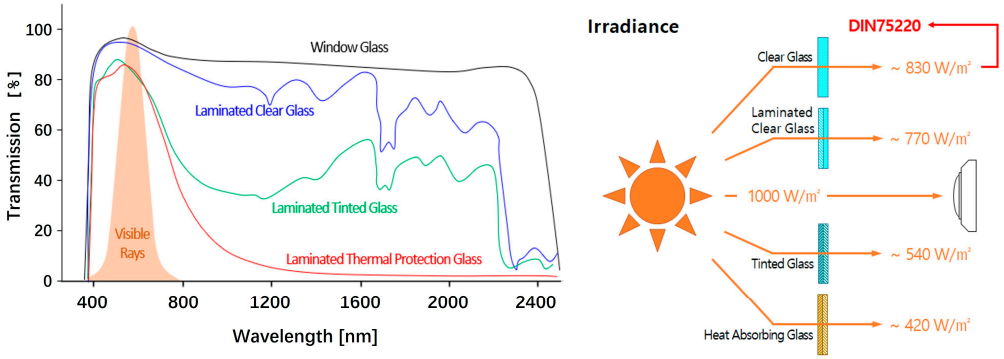

Figure 3. Reduced wavelength and solar radiation by type of glass [27].

Unlike the low-ferrous glass used in PVs, automobile glass uses reinforcing normal flat glass; therefore, the wavelength and solar irradiation transmitted through the surface reflection and absorption of the glass decrease. The reflection and absorption decreased more in the ultraviolet region below 400 nm. The low-ferrous tempered glass used in the PV module has a transmittance of approximately 92%, and the transmittance is increased to approximately 95% in the visible light region using low-reflectance coating. If the combined light test is applied to a PV module, the wavelength conditions should be strengthened,

such as the outdoor conditions of DIN 75220 and IEC 60068-2-5 (Simulated Solar Radiation at the Ground Level and Guidance for Solar Radiation Testing and Weathering). The DIN 75220 test standard was used to confirm the feasibility of the combined light test. DIN 75220 was divided into a cycle test (Z) and a long-term test (D), depending on the exposure area. A long-term test was performed under six long-term light irradiation conditions with 240 h of irradiation. The cycle test was conducted under repeated dry and humid conditions, as shown in Figure 4. It consisted of outdoor cycle tests 1 and 2 and indoor cycle tests 1 and 2.

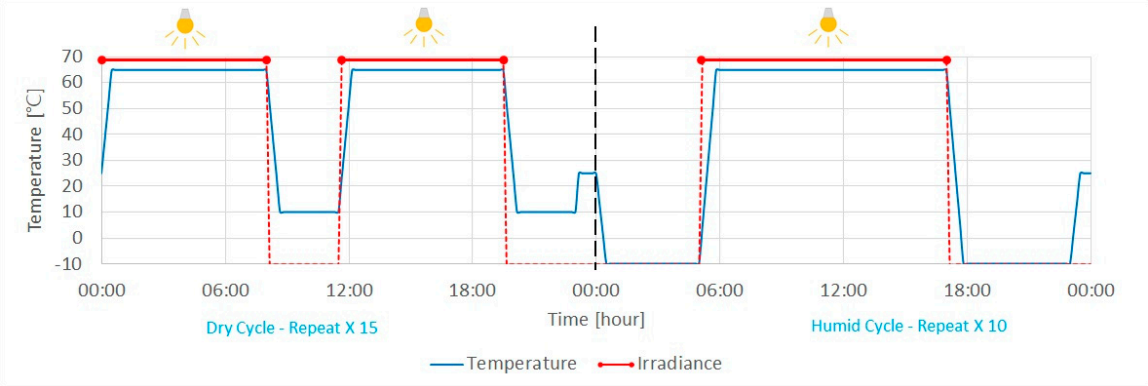

Figure 4. Temperature cycle of dry condition (left) and humid condition (right) in DIN 75220 [28].

In the PV modules, indoor cycle test 2 was applied among the cycle tests. It consisted of a dry climate cycle, which took 24 h and was repeated 15 times, and a humid climate cycle, which took 24 h and was repeated 10 times. The dry and humid climate cycles consisted of the following steps:

Indoor cycle test 1—dry climate cycle

- Daytime dry climate: 8 h
- Nighttime dry climate: 3.5 h
- Daytime dry climate: 8 h
- Nighttime dry climate: 3.5 h
- Room condition for inspection, re-building, maintenance: 1 h

Indoor cycle test 2—humid climate cycle

- Nighttime frost climate: 5 h
- Daytime humid climate: 12 h
- Nighttime frost climate: 6 h
- Room condition for inspection, re-building, maintenance: 1 h

The test conditions for the dry cycle were 10–65 °C, 30–55% RH, 830 W/m^2, and 12 h of irradiation time in each cycle.

Figure 5 shows the performance of the bifacial and shingled PERC solar modules under accelerated aging conditions, as determined by the DIN 75220 test.

Figure 6 shows the chamber used for the IEC 61215 and DIN 75220 tests. This chamber is capable of simulating solar irradiance (1 sun) and can adjust the ambient temperature from −40 °C to +90 °C. It also has the ability to control relative humidity between 25% and 80%. This chamber is used as a measuring device in KOLAS (Korea Laboratory Accreditation Scheme) accredited testing, and it undergoes regular calibration once a year. Table 4 summarizes the calibration results.

Figure 5. DIN 75220 test chamber environment (left: bifacial module; right: shingled module).

Figure 6. Solar simulator chamber used for tests IEC 61215 and DIN 75220.

Table 4. Accuracy of the measuring instrument.

Setting Value	Measured Value	Indication	Correction	Uncertainty
40.0 °C/30% R.H.	29.2% R.H.	30% R.H.	−0.8% R.H.	3.7% R.H.
60.0 °C/70% R.H.	69.6% R.H.	70% R.H.	−0.4% R.H.	4.7% R.H.
80.0 °C/60% R.H.	58.1% R.H.	60% R.H.	−1.9% R.H.	4.6% R.H.
25 °C	26.5 °C	25 °C	1.5 °C	1.0 °C
60 °C	29.9 °C	60 °C	−0.1 °C	1.4 °C
90 °C	88.6 °C	90 °C	−1.4 °C	1.6 °C

The DIN 75220 test was conducted after light soaking, and the electrical characteristics were measured after dry and humid cycles, as shown in Figure 7.

Unlike the 2.48% drop rate of the high-temperature and high-humidity test and the 2.77% drop rate of the thermal cycling test, a higher drop rate with a value of 4.18% was observed. Table 5 lists the measured data for DIN 75220 and the output drop rate.

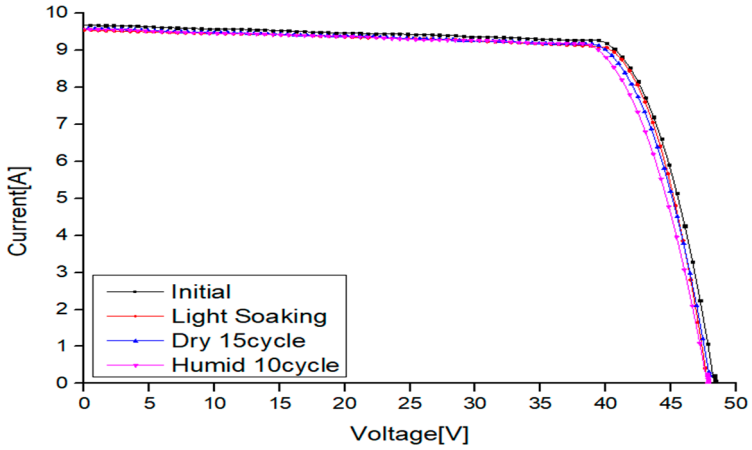

Figure 7. Measured data for DIN 75220.

Table 5. Measured data for DIN 75220 and output drop rate.

	Isc [A]	Voc [V]	Vpm [V]	Ipm [A]	Pm [W]	Rate 1 [%]	Rate 2 [%]
Initial	9.692	48.354	40.473	9.078	370.930	0.00	/
Light Soaking	9.674	48.318	40.229	9.025	368.349	−0.70	0.00
Dry 5 Cycle	9.664	48.219	40.017	9.136	365.593	−1.44	−0.75
Dry 10 Cycle	9.595	47.982	39.213	9.143	358.517	−3.35	−2.67
Dry 15 Cycle	9.591	48.079	39.769	9.005	360.359	−2.85	−2.17
Humid 5 Cycle	9.577	47.818	39.430	9.069	357.602	−3.59	−2.92
Humid 10 Cycle	9.564	47.797	39.211	9.008	355.419	−4.18	−3.51

Rate 1 in Table 6, which is the degradation rate compared with the initial measured value, is 2.05% lower than that of the IEC 61215 reliability test listed in Table 2. Rate 2 in the table represents the degradation rate relative to light soaking, and the output is approximately 2.72% lower than that in Table 2.

Table 6. Test matrix.

	IEC 61215 (DH)	IEC 61215 (TC)	DIN 75220	Difference (DH-DIN)
Initial Power [W]	372.132	371.741	370.930	1.202
After Light Soaking Rate 1 [%]	−2.48	−2.77	−3.59	1.11
Rate 2 [%]	−0.87	−1.32	−2.92	2.05
Final Power [W]	362.922	361.427	357.602	5.32

The DIN 75220 test, which simulates the environments of outdoor-parked vehicles degraded by solar light, temperature, and hot and humid conditions, is more likely to affect power degradation after light soaking than the high-temperature and high-humidity test, which tests degradation owing to humidity under a high temperature for an extended time, or the thermal cycling test, which evaluates the physical durability of the module through shrinkage and expansion.

3. Theoretical Model

The IEC 61215 standard presents limitations in accurately predicting the lifetimes of photovoltaic modules. In contrast, the DIN 75220 standard offers a more analytical approach. By subjecting the modules to accelerated stress conditions involving variations in irradiance, temperature, and humidity, DIN 75220 enables a more comprehensive assessment of module degradation. An energy balance model can be employed to accelerate lifetime predictions by calculating the latent heat of the module based on the energy balance of the system.

As shown in Figure 8, in photovoltaic modules, thermal energy is absorbed into tempered glass or polymer or is caused by various factors such as thermal equilibrium, thermodynamic loss, and resistance loss. Latent heat, which is the thermal energy accumulated in a PV module, is assumed to cause PV module deterioration in the actual environment. The latent heat was obtained using the energy balance equation, and the degradation ratio (DR_{mod}) was calculated.

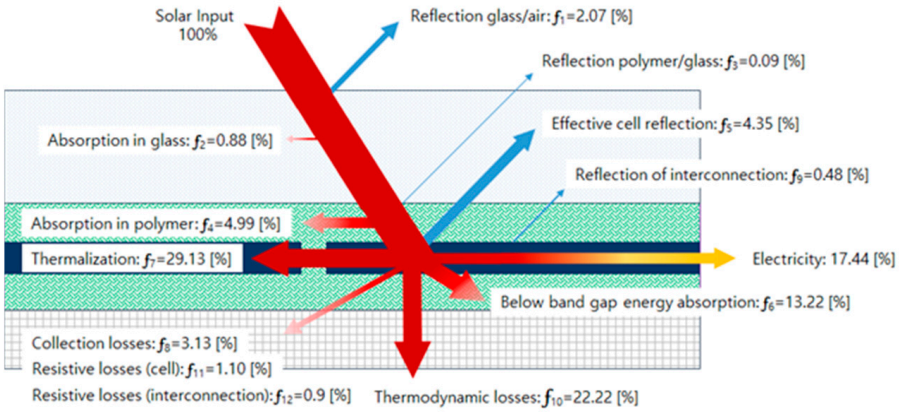

Figure 8. Contribution of heat and reflection loss and the rate of PV energy loss [29].

Table 7 lists the parameters required to obtain the latent heat of a PV module. Module-related data, such as the area, basic specifications of the module, absorption rate, environmental data in which the module operates, measurement data of the module, and latent heat, are required. The latent heat was calculated using Equation (1).

$$C_{mod} \times \frac{dT_{mod}}{dt} = q_{in} - P_{out} - q_{out} \quad (1)$$

Table 7. Parameters for the calculation of latent heat.

Module Data	Climate Data	Operating Data
Dimension	Irradiance	Output data
Rating	Ambient temperature	Module temperature
Absorbance or reflectivity	Relative humidity	-

The left side of (1) shows the specific heat (C_{mod}) and the change in temperature per hour (T_{mod}) for the PV module. The values calculated using this formula are the latent heat Q_{mod} and total heat energy remaining in the module [30]. The right side shows the total energy incident on the PV module (q_{in}), excluding the amount of power generation (P_{out}) and heat loss (q_{out}) of the PV module.

q_{in} is obtained using the absorbance, solar radiation of the solar panel, and area of the module. This represents the energy entering the PV module and can be expressed in (2).

A_{mod} is the area of the PV module, and R_{mod} is the reflectivity of the module. Reflectivity is a measure between 0 and 1, which indicates the proportion of light reflected by a surface. An object with a reflectivity of zero reflects all incident light, whereas an object with a reflectivity of one absorbs all incident light.

$$q_{in} = Irr_{measure} \times A_{mod} \times R_{mod} \tag{2}$$

P_{out} represents the output power of the solar module and is expressed by Equation (3).

$$P_{out} = \left(P_{max,STC} - P_{temp}\right) \times \left(\frac{Irr_{measure}}{Irr_{STC}}\right) \tag{3}$$

In (3), $P_{max,STC}$ is the power generation in standard test conditions (STCs). The reduction in the temperature of the module (P_{temp}) is subtracted from $P_{max,STC}$ and multiplied by the ratio of the measured insolation ($Irr_{measure}$) to the insolation in STCs (Irr_{STC}).

q_{out} is the heat emitted from the module via convection. It can be obtained using the thermal capacity of the module (C_{mod}), the convection coefficient (δ), and the temperature difference between the module and the atmosphere (ΔT) and is expressed in (4).

$$q_{out} = \delta \times \Delta T \times C_{mod} \tag{4}$$

The thermal capacity of a PV module varies with the constituent material. In this study, the general thermal capacity suggested by [30] and the thermal conductivity proposed by [31] were used.

The latent heat, denoted as $C_{mod} \times \frac{dT_{mod}}{dt}$ in Equation (1), is referred to as Q_{mod}. Q_{mod} is calculated using Equations (1)–(4). We analyzed the extent to which it contributed to the deterioration of the PV modules using the calculated Q_{mod} and the measured results from the DIN 75220 test.

The Q_{mod} of the dry cycle was 991 W, and the Q_{mod} of the humid cycle was 1093 W. The DIN 75520 standard prescribes a dry cycle of 240 h and a humid cycle of 120 h, both under an irradiance of 830 W/m^2. To calculate the energy balance model, the cumulative solar irradiance incident on a solar module must be quantified. This necessitates the conversion of irradiance from standard test conditions (STCs). In this study, the cumulative irradiance under STCs is termed the irradiation time and is quantitatively determined using Equation (5). The insolation times become 199.2 h and 99.6 h each if they are translated into STCs using Equation (5).

$$\text{Irradiation time} = \frac{Irr \times Time_{Irr} \times Cycle_{count}}{Irr_{STC}} \tag{5}$$

Table 8 lists the irradiation time, degradation rate, and accumulated latent heat of each process in DIN 75220. The accumulated latent heat and accumulated degradation rate increase as the process progresses. This means that there is a correlation between the latent heat and deterioration of the PV module. The hours for Q_{10y} and Q_{25y} were calculated by applying the average power generation time at the location tested, which is 3.05 h. The degradation ratio of the PV module according to accumulated latent heat is represented in Figure 8, and it was used to make a degradation equation.

Table 8. Results for the degradation ratio of the PV module calculated using latent heat.

	Irradiation Time [h]	Q_{mod} [W]	Q_T [Wh]	Degradation Rate (DR_{mod}) [%]	Degradation Ratio (P_R)
Initial ①	0	-	0	0	1
$Q_{DIN\ dry5}$ ②	66.4	991	65,802.33	1.44	0.9856
$Q_{DIN\ dry10}$ ③	132.8	991	131,604.7	3.35	0.9665
$Q_{DIN\ dry15}$ ④	199.2	991	197,407	2.85	0.9715
$Q_{DIN\ humid5}$ ⑤	249.0	1093	251,838	3.59	0.9641
$Q_{DIN\ humid5}$ ⑥	298.8	1093	306,269	4.18	0.9582
$Q_{DIN\ 10y}$ ⑦	11,132.50	1042	11,600,065.0	8	0.92
$Q_{DIN\ 25y}$ ⑧	27,831.25	1042	29,000,162.5	17	0.83

Figure 9 shows the power output reduction due to latent heat at each stage using the degradation rate of the module. DR_{mod} point ① is the initial output when DR_{mod} is 0 and there is no deterioration of the PV module. Points ②, ③, and ④ are the degradation rates after 5, 10, and 15 dry cycles each. Points ⑤ and ⑥ are the degradation rates after 5 and 10 humid cycles each. Points ⑦ and ⑧ are the deterioration rates 10 and 25 years after installation guaranteed by the module manufacturers. Based on these results, (6) is proposed, motivated by the sigmoid function [32]. To interpret the output of the PV module with the latent heat remaining in the module, the output power ratio P_R is introduced to reflect the power performance of the module with time, and it is represented by (6) using the coefficients in Table 9.

$$P_R = 1 + \alpha \cdot d - \frac{a}{b + \exp\left(-\frac{c}{Q_T}\right)} \tag{6}$$

$$DR_{mod} = 1 - P_R \tag{7}$$

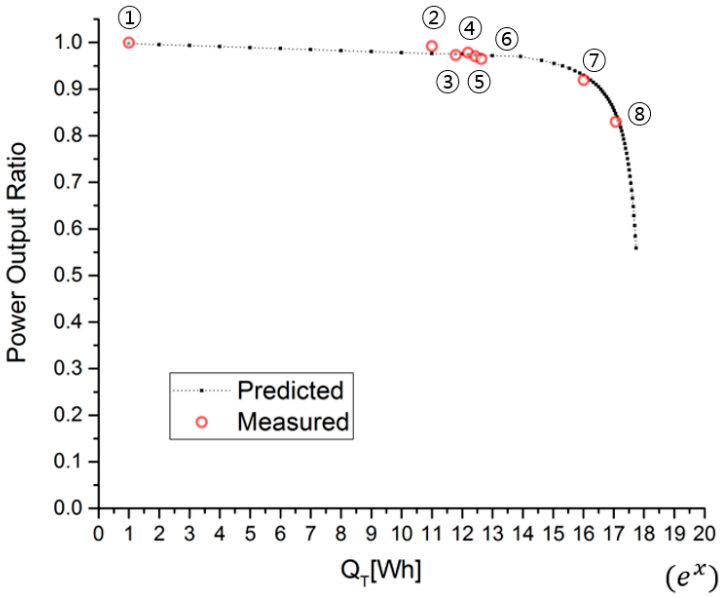

Figure 9. Power output ratio using deterioration rate of PERC module.

Table 9. Coefficients used for calculating output power ratio.

Coefficient	Value
a	−0.001916
b	−0.7685
c	4.771
d	0.007
α	0.357

In (6), d is the ratio of the output of the PV module, which is reduced by light irradiation. Because this varies with the PV module, coefficient α is used for compensation. The "a" coefficient affects the degradation rate, and if it increases, the degradation rate of the initial output increases. This coefficient is required because of the conditions that affect PV module deterioration, such as high temperature and high humidity. "b" is the coefficient that reduces degradation by wind speed and low ambient temperature. The "c" coefficient affects the sensitivity of the graph. Here, "Q_T" is a value obtained by integrating the latent heat of the PV module over the period of PV module installation by taking the natural logarithm of the heat quantity integration. The degradation rate of the PERC module due to latent heat can be calculated using Equation (7).

The fitting accuracy of (6) is 0.0693 in terms of root-mean-square error. Equation (6) can predict P_R by calculating the duration of module installation, the amount of insolation, and the environmental data of the installation location. The accumulated heat can be calculated by substituting (6) into (8) when P_R is known.

$$Q_T = \exp\left[-\frac{c}{\ln\left(\frac{a}{-P_R+\alpha\cdot d+1} - b\right)}\right] \tag{8}$$

The lifespan of the PV module can be predicted using Q and is expressed as (9).

$$Q_{mod\_lifetime}(expected\ PV\ module\ life\ time) = \frac{Q_T}{Q_{yr}} \tag{9}$$

When a power drop occurs during degradation, Q_T can be obtained using (8), and the expected lifetime of the module can be calculated by dividing by the amount of heat accumulated per year. The lifetime of the module can be predicted by calculating P_R using (6)–(9).

Table 10 compares the installation environments of land-based solar power plants and offshore solar power plants. It is observed that solar panels installed for marine PVs have lower module temperatures due to the cooler ambient conditions. A natural environment that is advantageous for the lifetime of a PV module can be predicted using experimental data and this model. The deterioration rate was calculated by comparing the general rooftop PV and marine PV systems with chamber experiments. DIN75220's dry cycle result was used as the theoretical lifetime. The data of the module installed on the rooftop of the campus (37°32′29.1″ N 127°04′46.7″ E) were used as the lifetime of the PV on land, and the data of the module installed in the sea of Gunsan (35°56′03.6″ N 126°31′36.4″ E) were used as the lifetime of the marine PV.

Table 10. Comparison of installation environments between land-based solar and marine solar PVs.

	Roof Top PV	Marine PV
Irradiation Time [h]	3.05	3.05
Ambient Temperature [°C]	15.98	14.64
Module Temperature [°C]	16.83	15.1
Relative Humidity [%]	41.31	41.28

Figure 10 shows the module and ambient temperature data from Gunsan and the campus rooftop. Based on these data, the ambient temperature of the rooftop PV was always 1–2 °C higher than that of the marine PV, except in August, September, and November. In addition, the module temperature of the rooftop was always higher than that of the marine PV.

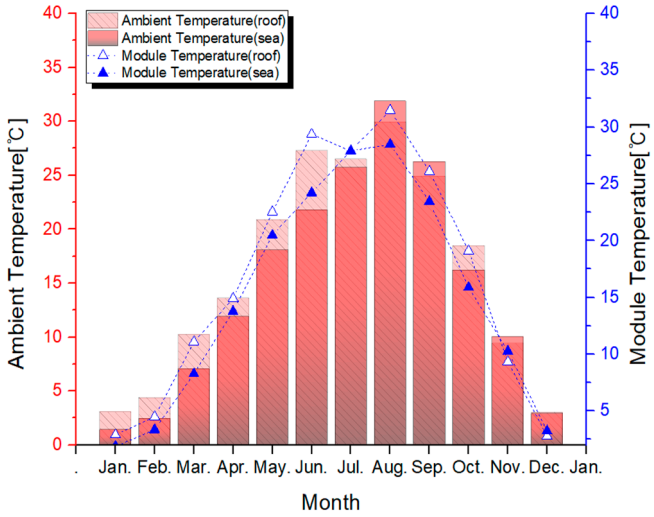

Figure 10. Comparisons of module and ambient temperature of Gunsan and campus rooftop (test site).

Figure 11 shows the calculated life expectancy of the PERC module used in the experiment. To verify this, an initial power reduction experiment was conducted. PV modules were installed outdoors for one week and six months to measure the reduction in power owing to natural light. After one week, the output power decreased by less than 1%, and it was less than 2.7% after six months of the experiment. This output reduction was caused by the initial LID. Therefore, the proposed model can reflect a reduction in the initial power. In addition, the data presented by PV module manufacturers were validated, confirming that the model can calculate short- and long-term output reductions.

Here, Q_T of the rooftop PV system was higher than that of the marine PV system owing to the characteristics of the module temperature. Thus, the latent heat in the module accelerated the degradation of the PV module. The values obtained by the model match the guaranteed output reduction value from the PV module manufacturers and 2–3% LID. Marine PVs are expected to have a life expectancy approximately three years more than the theoretical life expectancy, and four years more than rooftop PVs.

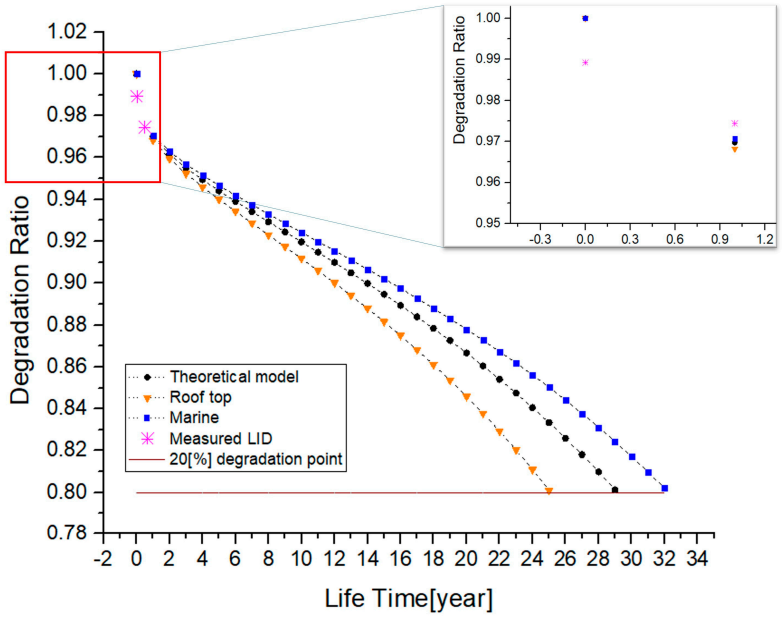

Figure 11. Life prediction of PERC module according to installation location using thermal energy.

4. Conclusions

Long-term reliability tests of PV modules were conducted in accordance with IEC 61215 standards. However, IEC 61215 cannot properly assess the long-term reliability of high-power-density PV modules, such as PERCs. The serial connections of the full cell gradually decreased during the manufacturing process. Moreover, connections in series and in parallel made by dividing and integrating solar cell methods, such as half-cut, shingling, and gapless methods, increased. Therefore, the PV module operated at a higher temperature than the full-cell module in the same environment. When the operating temperature of a module increases, the life expectancy of the polymer material in the module decreases, which can cause LID. However, to verify this, an LeTID test added to IEC 61215:2019 was conducted. Because PV modules are manufactured using various materials, each element can be evaluated individually. However, it is insufficient to verify PV modules with temperature and humidity (damp heat, humidity freeze), temperature change (thermal cycling), and light source and temperature (LeTID). A light-combined damp heat cycle test should be conducted. The conditions for the light-combined damp heat cycle test were set and tested similarly to those of DIN 75220.

In addition, it is necessary to verify whether this test induces the deterioration of the PV modules with appropriate stress. The concept of Q_{mod} was defined for this purpose. The Q_{mod} formula can verify how the lifetime of a PV module changes depending on the amount of latent heat possessed by the module. The accuracy of the fit of the life prediction curve of the product guaranteed by the PV module manufacturers can be determined by calculating the latent heat generated by the module according to the light-combined damp heat cycle test. Using this Q_{mod} concept, the lifespan of a PV module can be predicted based on the environmental factors of the actual installation area. By predicting the lifespan of actual PV modules in rooftop and sea environments using Q_{mod}, we determined that the marine PV system could be used longer than the rooftop PV system, assuming that latent heat is the only cause of deterioration. Therefore, module life depends on whether the latent heat of the module is emitted. Because the temperature of modules in floating and marine environments is lower than that of modules on land and rooftops, floating and marine PVs can emit latent heat more easily. This is advantageous for extending the life of the module and improving power generation efficiency.

Author Contributions: Conceptualization and methodology, W.N.; investigation and data curation, J.C., G.K., and J.H.; writing—original draft preparation, W.N. and J.C.; supervision, H.A.; review and editing, H.A. and N.P. All authors have read and agreed to the published version of the manuscript.

Funding: This research received no external funding.

Data Availability Statement: The original contributions presented in the study are included in the article; further inquiries can be directed to the corresponding author.

Acknowledgments: A preliminary version of this paper has been published in part in the Ph.D. dissertation of Woo Jun Nam [32].

Conflicts of Interest: The authors declare no conflicts of interest.

References

1. Green, M.A.; Blakers, A.W.; Kurianski, J.; Narayanan, S.; Shi, J.; Szpitalak, T.; Taouk, M.; Wenham, S.R.; Willison, M.R. *Ultimate Performance Silicon Solar Cells*; Final Report, NERDDP Project 81/1264 (Jan. 1982–Dec. 1983); Department of Resources and Energy: Canberra, Australia, 1984.
2. Chiang, C.J.; Richards, E.H. A 20 Percent efficient photovoltaic concentrator module. In Proceedings of the 21st IEEE Photovoltaic Specialists Conference, Kissimimee, FL, USA, 21–25 May 1990; Volume 2, pp. 861–863. [CrossRef]
3. Fischer, H.; Pschunder, W. Investigation of photon and thermal induced changes in silicon solar cells. In Proceedings of the 10th IEEE PVSC, Palo Alto, CA, USA, 13–15 November 1973; Volume 10, pp. 404–411.
4. Lindroos, J.; Savin, H. Review of light-induced degradation in crystalline silicon solar cells. *Sol. Energy Mater. Sol. Cells* **2016**, *147*, 115–126. [CrossRef]
5. Herguth, A.; Schubert, G.; Kaes, M.; Hahn, G. A New Approach to Prevent the Negative Impact of the Metastable Defect in Boron Doped CZ Silicon Solar Cells. In Proceedings of the 2006 IEEE 4th World Conference on Photovoltaic Energy Conference, Waikoloa, HI, USA, 7–12 May 2006; Volume 1, pp. 940–943. [CrossRef]
6. Fokuhl, E.; Philipp, D.; Mülhöfer, G.; Gebhardt, P. LID and LETID evolution of PV modules during outdoor operation and indoor tests. *EPJ Photovolt.* **2021**, *12*, 6, EU PVSEC 2021: State of the Art and Developments in Photovoltaics. [CrossRef]
7. Schmidt, J.; Aberle, A.G.; Hezel, R. Investigation of carrier lifetime instabilities in CZ-grown silicon. In Proceedings of the 26th IEEE Photovoltaic Specialists Conference, Anaheim, CA, USA, 29 September–3 October 1997; pp. 13–18. [CrossRef]
8. Fertig, F.; Lantzsch, R.; Mohr, A.; Schaper, M.; Bartzsch, M.; Wissen, D.; Kersten, F.; Mette, A.; Peters, S.; Eidner, A.; et al. Mass production of p-type Cz silicon solar cells approaching average stable conversion efficiencies of 22%. *Energy Procedia* **2017**, *124*, 338–345. [CrossRef]
9. Niewelt, T.; Selinger, M.; Grant, N.E.; Kwapil, W.; Murphy, J.D.; Schubert, M.C. Light-induced activation and deactivation of bulk defects in boron-doped float-zone silicon. *J. Appl. Phys.* **2017**, *121*, 185702. [CrossRef]
10. Sio, H.C.; Wang, H.; Wang, Q.; Sun, C.; Chen, W.; Jin, H.; Macdonald, D. Light and elevated temperature induced degradation in p-type and n-type cast-grown multicrystalline and mono-like silicon. *Sol. Energy Mater. Sol. Cells* **2018**, *182*, 98–104. [CrossRef]
11. Chen, D.; Hamer, P.G.; Kim, M.; Fung, T.H.; Bourret-Sicotte, G.; Liu, S.; Chan, C.E.; Ciesla, A.; Chen, R.; Abbott, M.D.; et al. Hydrogen induced degradation: A possible mechanism for light- and elevated temperature- induced degradation in n-type silicon. *Sol. Energy Mater. Sol. Cells* **2018**, *185*, 174–182. [CrossRef]
12. Ramspeck, K.; Seidl, A.; Birkmann, B.; Gassenbauer, Y.; Metz, A.; Nagel, H.; Zimmermann, S. Light Induced Degradation of Rear Passivated mc-Si Solar Cells. In Proceedings of the 27th European Photovoltaic Solar Energy Conference, Frankfurt, Germany, 24–28 September 2012; pp. 861–865. [CrossRef]
13. Zuschlag, A.; Skorka, D.; Hahn, G. Degradation and regeneration in mc-Si after different gettering steps. *Prog. Photovolt. Res. Appl.* **2017**, *25*, 545–552. [CrossRef]
14. Bredemeier, D.; Walter, D.C.; Schmidt, J. Possible Candidates for Impurities in mc-Si Wafers Responsible for Light-Induced Lifetime Degradation and Regeneration. *Solar RRL* **2017**, *2*, 1700159. [CrossRef]
15. Eberle, R.; Kwapil, W.; Schindler, F.; Schubert, M.C.; Glunz, S.W. Impact of the firing temperature profile on light induced degradation of multicrystalline silicon. *Phys. Status Solidi Rapid Res. Lett.* **2016**, *12*, 861–865. [CrossRef]
16. Fischer, M.; Woodhouse, M.; Herritsch, S.; Trube, J. *International Technology Photovoltaic Roadmap (ITRPV)*; VDMA Photovoltaic Equipment: Frankfurt am Main, Germany, 2020. Available online: https://resources.solarbusinesshub.com/images/reports/248.pdf (accessed on 1 January 2025).
17. Yoshikawa, K.; Kawasaki, H.; Yoshida, W.; Irie, T.; Konishi, K.; Nakano, K.; Uto, T.; Adachi, D.; Kanematsu, M.; Uzu, H.; et al. Silicon heterojunction solar cell with interdigitated back contacts for a photoconversion efficiency over 26%. *Nat. Energy* **2017**, *2*, 17032–17039. [CrossRef]

18. Bao, S.J.; Yang, L.Y.; Huang, J.; Bai, Y.H.; Yang, J.; Wang, J.L.; Lu, L.F.; Feng, L.; Bai, X.L.; Ren, F.Y.; et al. The rapidly reversible processes of activation and deactivation in amorphous silicon heterojunction solar cell under extensive light soaking. *J. Mater. Sci. Mater. Electron.* **2021**, *32*, 4045–4052. [CrossRef]
19. Chavali, R.V.K.; De Wolf, S.; Alam, M.A. Device physics underlying silicon heterojunction and passivating-contact solar cells: A topical review. *Prog. Photovolt. Res. Appl.* **2018**, *26*, 241–260. [CrossRef]
20. Tao, Y.G.; Upadhyaya, V.; Jones, K.; Rohatgi, A. Tunnel oxide passivated rear contact for large area n-type front junction silicon solar cells providing excellent carrier selectivity. *AIMS Mater. Sci.* **2016**, *3*, 180–189. [CrossRef]
21. Feldmann, F.; Bivour, M.; Reichel, C.; Hermle, M.; Glunz, S.W. Passivated rear contacts for high-efficiency n-type Si solar cells providing high interface passivation quality and excellent transport characteristics. *Sol. Energy Mater. Sol. Cells* **2014**, *120*, 270–274. [CrossRef]
22. Lu, M.; Mikeska, K.R.; Ni, C.; Zhao, Y.; Chen, F.; Xie, X.; Zhang, C. Screen-Printable Conductor Metallizations for Industrial n-TOPCon Crystalline Silicon Solar Cells. In Proceedings of the 2021 IEEE 48th Photovoltaic Specialists Conference (PVSC), San Juan, Puerto Rico, 20–25 June 2021; pp. 954–957.
23. VDMA Photovoltaic Equipment. *International Technology Roadmap for Photovoltaic (ITRPV)*, 15th ed.; VDMA Photovoltaic Equipment: Frankfurt am Main, Germany, 2024. Available online: https://www.vdma.org/international-technology-roadmap-photovoltaic (accessed on 1 January 2025).
24. *IEC 61215-1-1*; Terrestrial Photovoltaic (PV) Modules—DESIGN Qualification and Type Approval—Part 2: Test Procedures, 2016 ED 1. International Electrotechnical Commission: Geneva, Switzerland, 2016.
25. *IEC 61215-2*; Terrestrial Photovoltaic (PV) Modules—Design Qualification and Type Approval—Part 2: Test Procedures, 2019 ED 2. International Electrotechnical Commission: Geneva, Switzerland, 2019.
26. *DIN 75220*; Ageing Automobile Components in Solar Simulation Units. MaTestLab: New Castle County, DE, USA, 1992.
27. Burkhard, S. Light and Radiation Techniques for Airbag System Testing. K.H. Steuernagel Lichttechnik GmbH. Available online: https://www.yumpu.com/en/document/view/37573018/light-and-radiation-techniques-for-airbag-system-crash-network (accessed on 10 January 2025).
28. Zielnik, A.; Reidl, A.; Senff, S. The Principles of Weathering and How They Apply to Environmental Durability Testing of PV Backsheets. In Proceedings of the 3rd Atlas NIST Workshop on Photovoltaic Materials Durability, Gaithersburg, MD, USA, 8–9 December 2015. Available online: https://www.nist.gov/system/files/documents/el/building_materials/Applying-the-Fundamental-Principles-of-Weathering-to-Environmental-Durability-Testing-of-PV-Backsheets-Allen-Zielnik.pdf (accessed on 1 January 2025).
29. Hanifi, H.; Pfau, C.; Turek, M.; Schneider, J. A practical optical and electrical model to estimate the power losses and quantification of different heat sources in silicon based PV modules. *Renew. Energy* **2018**, *127*, 602–612. [CrossRef]
30. Jone, A.D.; Underwood, C.P. A thermal model for photovoltaic systems. *Sol. Energy* **2001**, *70*, 349–359. [CrossRef]
31. Choi, J.H.; Hyun, J.; Lee, W.; Bhang, B.G.; Min, Y.K.; Ahn, H.K. Power Performance of High Density Photovoltaic Module Using Energy Balance Model under High Humidity Environment. *Sol. Energy* **2021**, *219*, 50–57. [CrossRef]
32. Nam, W.J. Degradation Rate of High Density Power PV Module Using Latent Heat Analysis of Concurrent Temperature and Humidity Cycles with Light Soaking. Ph.D. Thesis, Konkuk University, Seoul, Republic of Korea, 2021.